JOURNAL OF MECHANICAL ENGINEERING AND SCIENCES
ISSN: 2289-4659 e-ISSN: 2231-8380
VOLUME 17, ISSUE 4, 2023, 9689 – 9699
DOI: https://doi.org/10.15282/jmes.17.4.2023.3.0767

UNIVERSITI MALAYSIA PAHANG AL-SULTAN ABDULLAH

RESEARCH ARTICLE

Numerical study of piston bowl geometries on PFI-HCCI engine performance

M.N.M. Hafiz[1,2]*, A. A. Hairuddin[1], K.A. Md Rezali[1], S.U. Masuri[1], Muntasser A.A Mossa[1]

[1] Department of Mechanical and Manufacturing Engineering, Universiti Putra Malaysia, 43400, Serdang, Selangor, Malaysia
Phone: +60397696331; Fax: +60397697122
[2] Centre of Excellence for Technology and Engineering (CREaTE), Jabatan Kerja Raya Malaysia, 78000 Alor Gajah, Melaka, Malaysia

ABSTRACT - Homogeneous charge compression ignition (HCCI) is an advanced combustion strategy proposed to provide higher efficiency and lower emissions than conventional compression ignition. However, there are still tough challenges in the successful operation of HCCI engines. Among these challenges, homogeneous mixture preparation and combustion phase control plays a vital role in determining the efficiency and emissions. Piston bowl geometry significantly enhances the process by improving the flow, turbulence, and mixing for the combustion. The study utilised experimental and numerical simulation methods to analyse HCCI combustion in port fuel injection (PFI) mode and evaluate the effect of piston geometries on engine performance. For this purpose, the different pistons bowl geometries (Baseline model, SQC, and CCC) with the same volume, compression, and equivalence ratio were numerically tested in a four-stroke, single-cylinder, YANMAR diesel engine. The numerical simulation results provide adequate assurance to proceed with the study with different piston geometries design. Compared to SQC and CCC, the Baseline model produced significantly higher cylinder pressure, temperature, and heat release rate. Different piston shape designs influenced the formation of air-fuel mixing, thereby affecting the time and location of onset combustion. The present investigation offered the significant role of piston geometry for the control mechanism of PFI-HCCI combustion, that is a vital part in demonstrating HCCI combustion.

ARTICLE HISTORY
Received : 13th Feb. 2023
Revised : 07th Sept. 2023
Accepted : 20th Nov. 2023
Published : 26th Dec. 2023

KEYWORDS
HCCI
Diesel
Piston bowl
Piston crown
Port fuel injection
Computational fluid dynamics
Internal combustion engine

1.0 INTRODUCTION

Internal combustion engines are the predominant source of power in the transportation industry. The development of the automobile industry and the increase in the number of vehicles have escalated the risk of fossil-derived fuels depletion and pushed exhaust gas emissions to critical levels [1–4]. Numerous combustion approaches have been studied to fulfil future requirements for clean and efficient combustion engines. Most of the current strategies fall within low-temperature combustion (LTC). LTC is the preferred NOX reduction that requires high activation energy [5–7]. In this regard, the homogeneous charge compression ignition (HCCI) combustion mode has the potential [8–12]. HCCI engine is a promising technology in engine research due to its capability to increase thermal efficiency while maintaining low emissions. It may be implemented by altering either SI or CI engines [13]. Significant progress has been made in the three main research fields of HCCI: fundamental theory, gasoline-fuelled HCCI combustion and diesel-fuelled HCCI combustion.

Among the fuels, gasoline has high volatility; thus, evaporation is rapid, and a premixed charge can be obtained using port fuel injection. Gasoline, however, is resistant to auto-ignition; it becomes difficult to achieve combustion at low-load conditions [14, 15]. On the other hand, diesel fuel has superior auto-ignition qualities compared to gasoline. Diesel fuel has significant cool-combustion chemistry, it will lead to rapid auto-ignition once compression temperatures exceed about 800 K [16]. However, there are still tough challenges in the successful operation of HCCI engines for diesel fuel, such as controlling the combustion phasing, extending the operating range, and high unburned hydrocarbon and CO emissions [17]. Preparing a homogeneous mixture in diesel is difficult due to the lower volatility, higher viscosity and lower resistance to auto-ignition. The process requires elevated temperatures before vaporization occurs in order to form a premixed homogeneous charge. The essential factor needed to achieve in diesel HCCI combustion is mixture control, including charge components, temperature control in the whole combustion history, and high pre-ignition mixing rates [15].

It has been widely proven in the literature that the geometry of the piston bowl can affect flow, turbulence, mixing and combustion in an engine [18–24]. Any improvement in fuel-air mixing inside the cylinder can significantly enhance combustion, raising engine performance and reducing emissions [25]. In-cylinder gas flow is governed primarily by the fluid's swirl and turbulent kinetic energy, resulting in flame propagation inside the cylinder [26]. Although there are numerous ways to increase the airflow within a diesel engine's cylinders, the combustion chamber's design has been of particular interest to researchers over the past decade. Rakopoulos et al. [27] examined the impact of piston bowl geometry and speed in a diesel-powered engine. According to their findings, the relationship between combustion chamber

*CORRESPONDING AUTHOR | N. M. Hafiz | ✉ nfia82@gmail.com

geometry, fuel injection, and gas flow is essential for defining combustion and emission characteristics. A key objective in designing the combustion bowl then is to ensure that mixing of fuel and air is adequate to mitigate the impact of fuel rich regions and allow the engine to meet its performance and emissions targets. In light-duty direct injection (DI) diesel engines, combustion chamber geometry influences the complex interactions between swirl and squish flows, spray-wall interactions as well as late-cycle mixing [28]. There are three principal classifications of pistons which are dome, flat, and bowl. The most common pistons in HCCI engines are bowl types, two-stroke pistons, dome-shaped pistons, and specialised pistons, each of which offers distinct advantages and disadvantages [29]. This circumstance has inspired researchers to investigate the beneficial impact of piston bowls on HCCI combustion engines in greater depth.

The complex internal combustion engine design has made employing an experimental study of the piston bowl's geometry hard. The study will be costly and time-consuming. On that note, numerical simulation has become a valuable tool for investigating and developing control strategies for the HCCI engine due to its higher flexibility and lower cost. The latest Computer Fluid Dynamic (CFD) software uses a highly efficient coupling of detailed chemical kinetics, liquid fuel spray and turbulent gas dynamics to simulate combustion processes in an internal combustion engine. Most studies on the piston geometry employed in CFD, however, have focused on CI engines [22, 30, 31]. Regarding HCCI, most studies do not emphasise on piston geometry design [32–35]. Therefore, it is essential to conduct a study utilising CFD techniques for HCCI engines since the engine offers several advantages in terms of emissions and performance.

In this study, HCCI combustion for a single-cylinder YANMAR L48N engine was numerically demonstrated by using ANSYS Forte. The effect of two basic piston bowls: cylinder combustion chambers (CCC) and square shape combustion chambers (SQC), on their combustion performance is then investigated. The results were analysed based on thermodynamic performance for their in-cylinder pressure, heat release rate, temperature, air flow and combustion period. Later in the future study, the improved design of these basic types will investigate further by modifying the bowl geometry.

2.0 METHODOLOGY

The research was carried out through experimental and numerical simulation. The experimental method has been used in a modified single-chamber Direct Injection Compression Ignition (DICI) engine to demonstrate the HCCI combustion and play a significant role in validating purposes. On the other hand, the numerical simulation approach has been employed to investigate the effect of different piston bowl geometries on engine performance.

2.1 Experimental Setup

The experiments were conducted on Yanmar L48N, a four-stroke single-cylinder, air-cooled, compression ignition (CI) diesel engine. The detailed specification is listed in Table 1. Preheating system is one of the control techniques to regulate the intake air temperature to switch the engine combustion to HCCI mode. For this case, an external air heater, a STANLEY-forced air heater, and Watlow heater 988A-20CC-CCRR were used to accommodate the heater pipe and control the intake manifold temperature. Besides that, a high-pressure 200-bar Volkswagen injector was connected to the same fuel pipeline with the current Diesel Injector (DI) and was used as Port Fuel Injection (PFI) combustion system. This technique, therefore, enables the PFI injector mechanism to work simultaneously with the DI injector (HCCI-DI) with the aid of an electronic computer unit (ECU) [36].

Various sensors and actuators were connected to the experimental engine, including an eddy current dynamometer, airflow meter, exhaust gas analyser, thermocouples, lambda sensor, and in-cylinder pressure sensor. An eddy current Tops Landtop dynamometer model, GFA174A-5, was used in the study. The dynamometer was then connected to its data logger and software to display and record speed, torque, and load data. Lambda (λ) sensor with a digital display uses an MTX-L digital air-fuel ratio gauge, and a Bosch heated wideband oxygen sensor located inside the exhaust gas pipe. The data of the air/fuel ratio was continuously obtained by the sensor at different engine loads during the engine operation. This study used two k-type thermocouples to monitor the engine and exhaust temperature; one was installed on the engine body close to the rotary blade, and another was installed next to the exhaust port. To complete the monitoring system, a pressure transducer Optrand model D5229-R41 was used to measure in-cylinder pressure. The sensor can measure pressure at a range from 0 to 5000 psi with a sensitivity of 0.84 mV/psi at 200°C. The transducer was connected to its own DAQ system to amplify the signal before it was read and sent to the computer. The schematic diagram of the engine setup is shown in Figure 1.

Table 1. Technical details of engine

Parameter	Description
Engine	YANMAR, L48N, single-cylinder
Cylinder bore	70 mm
Stroke length	58 mm
Compression ratio	20.1:1
Speed	2700 RPM
Injection system	DI and PFI (modified)

Table 1. (cont.)

Parameter	Description
Cooling system	Air
Fuel	Diesel
Equivalence Ratio	0.42
Exhaust valve close	385° CA
Intake valve open	335° CA
Intake valve close	559° CA

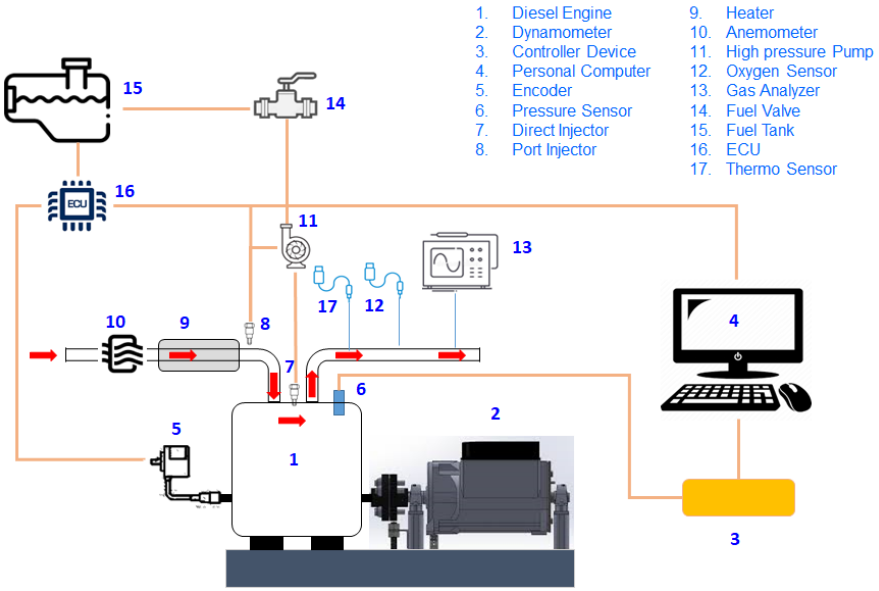

Figure 1. Schematic diagram for HCCI engine set-up

2.2 Simulation Setup

ANSYS Forte 2021 R2 (ANSYS Forte), a CFD software for internal combustion engine design applications, was used to model and simulate PFI-HCCI combustion for this study. The main structure of the thermo-fluids is directed by governing equations based on the conservation law of fluids' physical properties. ANSYS Forte applies a turbulent reacting flow representation in which the Navier-Stokes equations govern the basic fluid dynamics. Model transport equations of mass, momentum, and energy conservation laws are formulated for the compressible and gas-phase flows and represent the turbulent nature of the flow [37].

In this study, a series of numerical simulations was performed to demonstrate HCCI combustion in PFI mode and evaluate piston geometries' effect on engine performance. The simulation was conducted based on experimental works conditions in Table 1. A reduced n-heptane chemistry mechanism surrogates the diesel fuel for the simulation works. The chemistry file is a standard ANSYS Chemkin-Pro chemistry-set file containing 36 species and 74 reactions for a semi-detailed n-heptane model. This mechanism is validated based on fundamental experimental data for diesel engine operating conditions [38]. In addition, this study assumed the adiabatic wall boundary condition and constant temperatures were given to the walls, similar to the engine working conditions. Table 2 provides the set-up of initial conditions for this numerical study.

Table 2. Initial and boundary condition for numerical model

Parameter	Description
Cylinder head temperature	425 K
Liner temperature	375 K
Piston temperature	525 K
Initial pressure	1 Bar
Fuel	n-heptene
Fuel mass	0.0057g
Nozzle size (diameter)	0.0055 cm
Equivalence ratio, Ø	0.4

In addition to the original YANMAR L48N piston geometry, which serves as the baseline model, two other piston geometries, the cylinder combustion chamber (CCC) and the square shape combustion chamber (SQC), were chosen to compare their performance in PFI-HCCI combustion in mode. These models were chosen to investigate the fundamental combustion performance based on the shape of the basic piston geometry. Figure 2 depicts all three piston geometries. The results of this study include in-cylinder pressure, *p*, temperature, *T*, heat release rate (HRR), and turbulence kinetic energy (TKE). The best result will lead to the subsequent advanced investigation study.

(a) (b) (c)

Figure 2. Three piston bowl geometries used in numerical simulation: (a) baseline model, (b) CCC bowl and (c) SQC bowl

2.2.1 Fluid continuity equation

The gas-phase working fluids in CFD combustion are modelled as a mixture of individual gas species or components. This composition changes during the engine cycle due to molecular diffusion, flow convection, turbulent transport, interactions with fuel sprays, and combustion. The summation of the equation over all species gives the continuity equation for the total gas-phase fluid as Eq. (1).

$$\frac{\partial \bar{\rho}}{\partial t} + \nabla \cdot (\bar{\rho}\tilde{u}) = \dot{\rho}^s \tag{1}$$

where, ρ is density, $\tilde{u}$ the flow velocity vector and $\dot{\rho}^s$ is the source term due to spray evaporation.

2.2.2 Momentum conservation equation

The momentum equation for the fluid takes into account the effects of pressure force, convection, turbulent transport, viscous stress, liquid sprays, and body force. For ANSYS Forte, the equation is considered as follow:

$$\frac{\partial \bar{\rho}\tilde{u}}{\partial t} + \nabla(\bar{\rho}\tilde{u}\tilde{u}) = -\nabla\bar{p} + \nabla \cdot \bar{\sigma} - \nabla \cdot \Gamma + \bar{F}^s + \bar{\rho}\bar{g} \tag{2}$$

where, p is the pressure, F^s is the rate of momentum gain per unit volume due to the spray, g is the specific body force, σ is the viscous shear stress, and Γ is the stress that accounts for the effects of ensemble-averaging of the nonlinear convection.

2.2.3 Energy conservation equation

According to the First Law of Thermodynamics, the change in internal energy must be balanced by the pressure work and heat transfer. For flow issues associated with internal combustion engines, the effects of turbulent transport, convection, turbulent dissipation, sprays, chemical reactions, and enthalpy diffusion of a multicomponent flow must also be considered. The internal energy transport given in Eq. (3) as follows:

$$\frac{\partial \bar{\rho}\tilde{I}}{\partial t} + \nabla \cdot (\bar{\rho}\tilde{u}\tilde{I}) = -\bar{p}\nabla \cdot \tilde{u} - \nabla \cdot \bar{J} - \nabla \cdot H + \bar{\rho}\bar{\varepsilon} + \dot{\bar{Q}}^C + \dot{\bar{Q}}^S - \dot{\bar{Q}}_{rad} \tag{3}$$

where, I is the specific internal energy, J is the heat flux vector accounting for contributions due to heat conduction and enthalpy diffusion, $\bar{\varepsilon}$ is the dissipation rate of the turbulent kinetic energy, $\dot{\bar{Q}}^C$ and $\dot{\bar{Q}}^S$ are the rate of the turbulent kinetic energy due to chemical heat release and spray interactions, H accounts for the effects of ensemble-averaging or filtering of the convection, and $\dot{\bar{Q}}_{rad}$ is the radiative heat loss.

2.2.4 Gas-phase mixture equation of state

For the gas-phase mixture, the Equation of State relates to the thermodynamic properties of temperature, pressure, and density. The equation, then, also provides relations for the internal energy. The ideal gas law applies in ANSYS Forte, assuming the mixing gas components follow the Dalton model and be defined as Eq. (4) :

$$\bar{p} = R_u \bar{T} \sum_k \left(\frac{\bar{\rho}_k}{W_k}\right) \tag{4}$$

where, R_u is the universal gas constant, and W_k is the molecular weight of species k .

The internal energy of an ideal gas is only a function of temperature. The specific internal energy of the gas mixture ($\tilde{I}$) is a mass average of the specific internal energy of individual components ($\tilde{I}_k$), $\bar{y}_k$ is the mass fraction of species k, which are tabulated against temperature:

$$\tilde{I}(\bar{T}) = \sum_k \bar{y}_k \tilde{I}_k(\bar{T}) \tag{5}$$

2.2.5 Reynolds-Averaged-Navier-Stokes (RANS)

The simulation of an HCCI engine applies Navier-Stokes equations to govern the basic fluid dynamics. Turbulent flow is characterised by a wide range of flow length scales as well as large and irregular flow field fluctuations. The Reynolds-Averaged-Navier-Stokes (RANS) method, used for this study, aims to capture the ensemble average of the flow field from a vast number of flow realisations under similar conditions. Since turbulence affects fluid transport and mixing significantly more than laminar flow, the ensemble average of turbulent transport and mixing is identical to large-scale diffusion. The RANS technique eliminates the need to resolve small-scale structures and fluctuations in individual flow realisations while preserving the main effects of turbulence on averaged flow and combustion characteristics. In the RANS technique, the turbulent viscosity v_t is related to the turbulent kinetic energy $\tilde{k}$ and its dissipation rate $\tilde{\varepsilon}$, and the calculation of turbulent viscosity requires both to be modelled. The advanced version of the $\tilde{k} - \tilde{\varepsilon}$ model is derived from Re-Normalized Group (RNG) theory as given in Eq. (6) and Eq. (7) [39].

$$\partial \frac{\bar{\rho}\tilde{k}}{\partial t} + \nabla \cdot \left(\bar{\rho}\tilde{\boldsymbol{u}}\tilde{k}\right) = -\frac{2}{3}\bar{\rho}\tilde{k}\nabla \cdot \tilde{\boldsymbol{u}} + (\bar{\boldsymbol{\sigma}} - \boldsymbol{\Gamma}) : \nabla\tilde{\boldsymbol{u}} + \nabla \cdot \left[\frac{(\mu + \mu_T)}{Pr_k}\nabla\tilde{k}\right] - \bar{\rho}\tilde{\varepsilon} + \dot{\bar{W}}^S \tag{6}$$

and

$$\frac{\partial \bar{\rho}\tilde{\varepsilon}}{\partial t} + \nabla \cdot (\bar{\rho}\tilde{\boldsymbol{u}}\tilde{\varepsilon}) = -\left(\frac{2}{3}c_{\varepsilon 1} - c_{\varepsilon 3}\right)\bar{\rho}\tilde{\varepsilon}\nabla\tilde{\boldsymbol{u}} + \nabla.\left[\frac{(v + v_T)}{Pr_\varepsilon}\nabla\tilde{\varepsilon}\right] + \frac{\tilde{\varepsilon}}{\tilde{k}}\left[c_{\varepsilon 1}(\boldsymbol{\sigma} - \boldsymbol{\Gamma}) : \nabla\tilde{\boldsymbol{u}} - c_{\varepsilon 2}\bar{\rho}\tilde{\varepsilon} + c_s\dot{\bar{W}}^S\right] - \bar{\rho}R \tag{7}$$

In these equations, $Pr_k, Pr_\varepsilon, c_{\varepsilon 1}, c_{\varepsilon 2}, c_{\varepsilon 3}$ are model constants.

2.2.6 Chemical kinetics formulation

ANSYS Forte embedded Chemkin-Pro solver that can incorporate more extensive and accurate fuel models into a simulation. The Chemkin-Pro solver is used for chemical kinetic simulation, employing innovative and proprietary techniques to achieve remarkable calculation speeds. On that note, the Dynamic Cell Clustering application in the Chemkin-Pro leverages an advanced algorithm to group cells with similar kinetic conditions and eliminate duplicate calculations. Simultaneously, Dynamic Adaptive Chemistry will immediately and automatically lower the kinetics at each time step. Regarding the chemical kinetic mechanism, a simplified reduced n-heptane (nc7h16) mechanism was used in this study as a surrogate to diesel fuel. The chemistry file is a standard ANSYS Chemkin-Pro chemistry-set file, Diesel_1comp_35sp.cks file with 36 species and 74 reactions.

Chemical kinetic mechanisms can accurately describe the chemical reactions that occur in combustion simulations. These mechanisms define the reaction paths and the associated reaction rates that lead to the change in species concentrations. Consequently, the generic form in Eq. (8) can represent reversible or irreversible reactions involving chemical species in detailed chemical kinetic mechanisms [40].

$$\sum_{k=1}^{K} v'_{ki}\chi_k \Leftrightarrow \sum_{k=1}^{K} v''_{ki}\chi_{k(i=1,\ldots,i).} \tag{8}$$

whereby, the production rate of the k^{th} species in the i^{th} reaction can be written as

$$\dot{\omega}_{ki} = (v''_{ki} - v'_{ki})q_i(k = 1, \ldots, K) \tag{9}$$

where, q_i is the rate progress of rection i.

The summation of $\dot{\omega}_{ki}$ over all the reactions gives the chemical source term $\dot{\rho}_k^c$ in the species continuity equation as follow:

$$\dot{\rho}_k^c = W_k \sum_{i=1}^{I} \dot{\omega}_{ki} \tag{10}$$

Therefore, the chemical heat release term in the energy equation is denoted by Eq. (11) as follow:

$$\dot{Q}_c = -\sum_{i=1}^{I} Q_i\, q_i = \sum_{i=1}^{I}\sum_{k=1}^{K} (v''_{ki} - v'_{ki}) \left(\Delta h_f^0\right)_k q_i \tag{11}$$

where Q_i is heat of reaction of reaction i at absolute zero and $\left(\Delta h_f^0\right)_k$ is the heat of formation of species at absolute zero.

3.0 RESULTS AND DISCUSSION

3.1 Grid Independence Study

Ansys Forte employs on-the-fly cartesian volume mesh generation coupled with immersed boundary approach. The automatic mesh generation at each piston position depends on defined mesh-size criteria and specified mesh refinement settings. The Global Mesh Size sets the overall background mesh size, which is used everywhere when a mesh refinement is not defined. On the other hand, mesh refinement is utilised to resolve both surfaces and regions within the computational geometry where it has been specified. Moreover, Ansys Forte features an adaptive mesh solution that enables mesh refinement based on specific variables such as velocity and temperature [37]. All these mesh refinement options are activated at different periods and sizes according to needs. A smaller mesh size usually would yield a more accurate result. Nevertheless, there is a disadvantage: smaller mesh sizes demand more computational time and power. This consideration is essential as time and power resources are limited.

Mesh-sensitivity study has been conducted using four different grid resolutions with the same boundary and initial conditions. On that note, the global mesh sizes of 0.2cm and 0.3cm for cold flow simulation have been tested with and without refining. The details of the four mesh types and the corresponding computational runtime are shown in Table 3. Taken together, these results suggest that the mesh size of 0.3cm with refinement yielded the optimum accuracy and computational performance, therefore, was used in the subsequent simulations.

Table 3. Results obtained for grid independence study

Global Mesh Size	Max. numbers of cells	Max. Pressure (MPa)	Pressure Different	Runtime (hours)
0.2 Refinement	347,929	4.94	-	109.25 hours
0.3 Refinement	148,080	4.88	1.20%	36.15 hours
0.2 w/o refinement	112,924	4.86	1.62%	41.25 hours
0.3 w/o refinement	63,323	5.54	12.15%	20.25 hours

3.2 Model Validation

Figure 3 shows the comparison results of in-cylinder pressure and heat release rate (HRR) obtained for numerical simulation and experimental works. For experimental works, the average pressure data were obtained from the dynamometer, and the heat release rate was then determined by applying the first law of thermodynamics. As shown in Figure 3 numerical simulation model shows good agreement with the experimental data. The values of the peak in-cylinder pressure are predicted with less than 4% deviation from the experimental profile. In comparison, the heat release rate is predicted with a maximum error of approximately 2%. However, the timings of the peak heat release rate could be better predicted. The peak pressure and HRR are obtained at 3° bTDC for simulation as opposed to 5° bTDC for the experimental case. These results provide sufficient confidence for the present study.

Several factors could explain this observation. The discrepancy in in-cylinder pressure and heat release rate between numerical simulation data and experimental results can be attributable to two leading causes. The first is due to the assumptions made for the values of several engine specifications that were unavailable from the manufacturer and difficult to obtain. The second plausible cause for the discrepancy between simulation and experimental results is the assumptions made when developing the model, such as the boundary conditions. Since actual combustion chamber wall and piston surface temperatures could not be measured, values were derived using plausible estimates for normal operating conditions based on published literature.

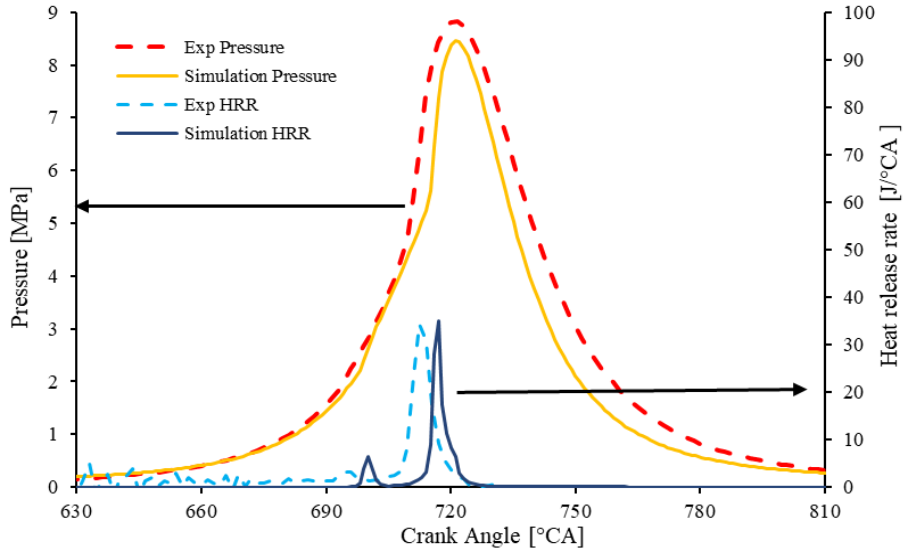

Figure 3. Comparison of in-cylinder pressure and heat release rate for experiment and numerical simulation

3.3 In-cylinder Pressure and Temperature

For an Internal Combustion Engine (ICE), in-cylinder pressure changes with crank angle due to changes in cylinder volume, combustion, and heat transfer to the cylinder wall. On top of this, the changes in cylinder volume and combustion contribute the most. The effect of a volume change on pressure can be easily demonstrated. As a result, information on the combustion rate can be derived from precise pressure measurements if models for the other phenomena can be created with the right level of approximation. For an internal combustion engine, the pressure increase caused by combustion is proportional to the amount of fuel chemical energy released, rather than being proportional to the mass of the mixture burned [26].

Figure 4 depicts the in-cylinder pressure and temperature obtained for three piston geometry designs. As presented in the numerical simulation results, comparing the three in-cylinder pressure reveals that Baseline geometry has the highest peak pressure, followed by SQC and CCC. The baseline model's maximum in-cylinder pressure was 8.46 MPa at 721° CA. Compared with the baseline model, the peak pressure for SQC piston geometry was 6.38 MPa at 726° CA and CCC as much as 6.22 MPa at 727° CA. As the volume of the cylinder decrease towards the TDC, the in-cylinder pressure for Baseline geometry significantly increases compared to CCC and SQC piston geometries. This scenario persists until the pressure is increased and the combustion is improved. This condition demonstrates that the Baseline piston geometry can release more fuel and chemical energy than other designs. This circumstance may be attributed to enhanced air-fuel mixing and swirling of air in the combustion chamber, which resulted in improved combustion [42, 43].

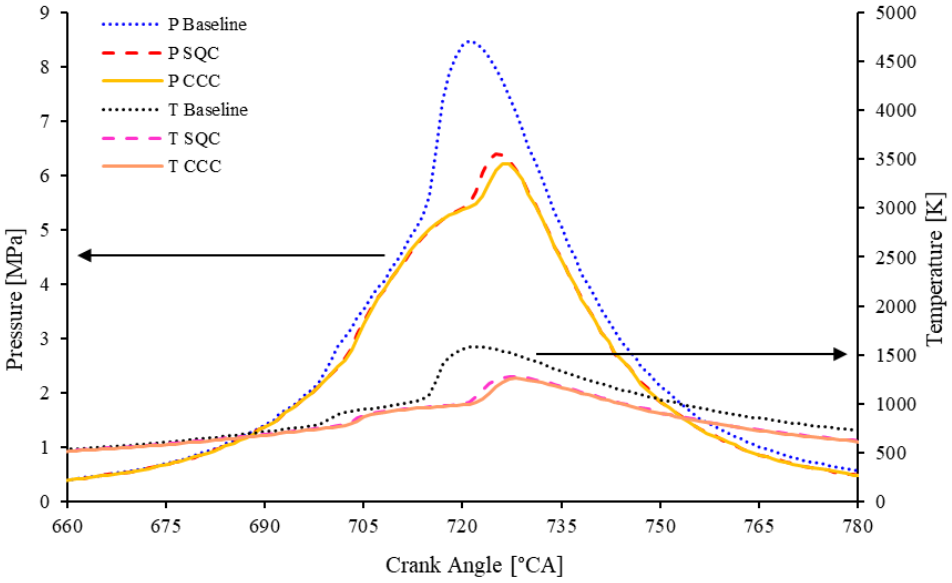

Figure 4. Comparison of in-cylinder pressure and temperature for different piston bowl geometries

Further analysis of in-cylinder temperature in Figure 4 reveals that the average temperature attained for the Baseline model is higher than for SQC and CCC, while the temperature for SQC is slightly higher than CCC. The differences in temperature in three different piston geometries are due to differing fuel stratification, which is related to the formation of the equivalent ratio [5]. The results also indicate that different piston geometry designs have affected the formation of equivalent ratios, thereby affecting the start of combustion (SOC). In addition to the in-cylinder temperature, Figure 5 depicts the onset timing of combustion and its location. It is understood that SOC for the Baseline model occurred earlier than SQC and CCC. The start of combustion for the Base model occurred at 715°CA in the middle right of the piston bowl, whereas the SQC and CCC occurred practically simultaneously at 720°CA at the bottom left of the piston bowl.

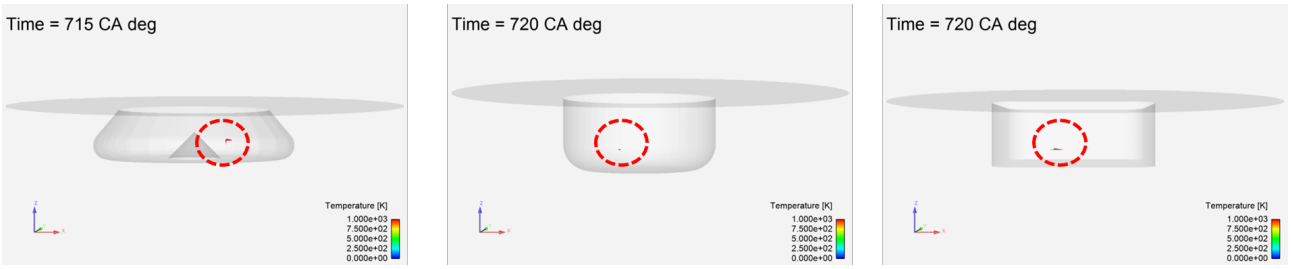

(a) (b) (c)

Figure 5. The location of combustion onset: (a) baseline, (b) CCC and (c) SQC

3.4 Rate of Heat Release Rate

Heat release rate (HRR), often called fuel combustion rate, is a method for determining the rate of chemical energy release from a fuel. Figure 6 compares the net heat release rate curves for three different piston geometry designs. It can be seen that the combustion of diesel fuels under HCCI exhibits a distinctive two-stage heat release. The first stage of the heat release curve is associated with low-temperature kinetic reactions. The time delay between the first and high-temperature kinetic reactions can be related to the "negative temperature coefficient (NTC) regime" that occurs between the two heat release stages. In this NTC regime, the total reaction rate decreases as the in-cylinder temperature increases, resulting in reduced system reactivity [17, 44].

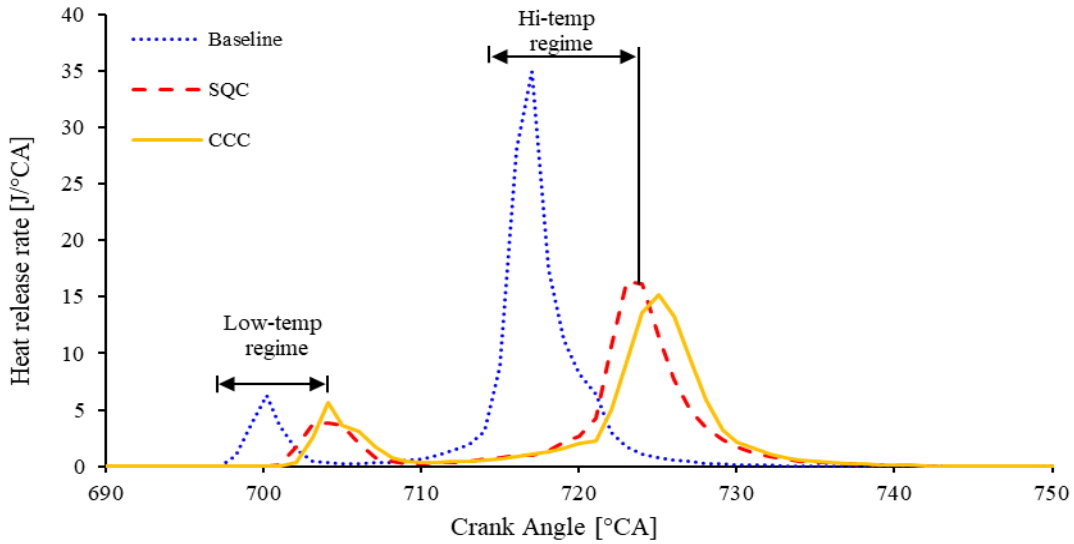

Figure 6. Comparison of heat release rate for different piston bowl geometries

Compared to the SQC and CCC piston geometries, HRR for the Baseline model geometry experiences combustion at the earliest stage. This condition holds true under both low-temperature and high-temperature circumstances. The baseline model had the highest HRR at 717° CA with 34.88 J/°CA, followed by SQC and CCC with HRR of 16.35 J/°CA and 15.50 J/°CA, respectively. The results are due to the improved air swirl motion in the Baseline combustion chamber compared to the SQC and CCC model, which leads to the mixing homogeneity of air-fuel, then improved combustion [42, 43]. Figure 7 depicted the airflow motion at 505°CA, immediately prior to the closure of the intake valve. From the figure, it can be determined that flow distribution occurred for the Baseline model was uniformly distributed. This condition prepared the Baseline model with sufficient air-fuel mixing and initiated the first stage of the heat release curve, which is associated with low-temperature kinetic reactions [44] . The condition allowed early SOC to occur in the Baseline model compared to the SQC and CCC model. Therefore, the design of piston bowl geometry for the Baseline model has played a crucial role in promoting better intake airflow during the injection period, thereby enhancing the combustion.

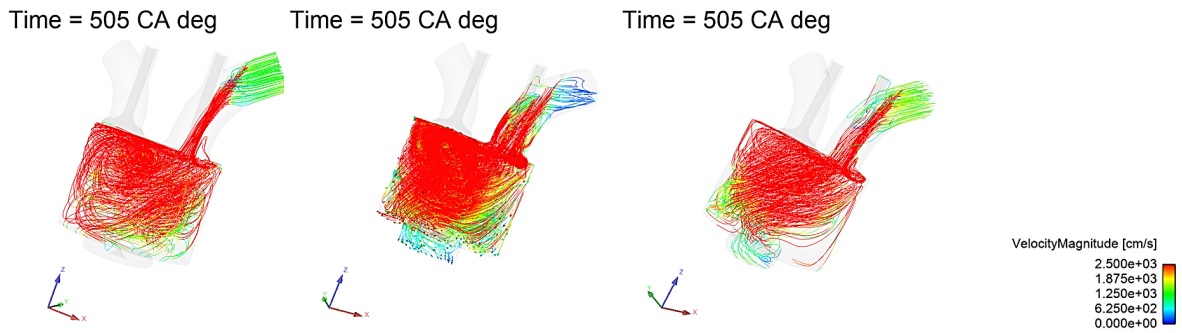

Figure 7. Air flow motion for different piston bowl geometries during intake flow

Figure 8 exhibits the cumulative heat release duration percentage for each of the three piston bowl shapes. The comparative result demonstrates that the heat release period from 10% to 90% (CA10-CA90; define CA) for the Baseline model was 19°CA, which was less than the duration for other piston bowl geometries. As depicted in the diagram, the combustion of SQC and CCC concludes after TDC, and it is presumed that these conditions contribute to pressure loss during combustion.

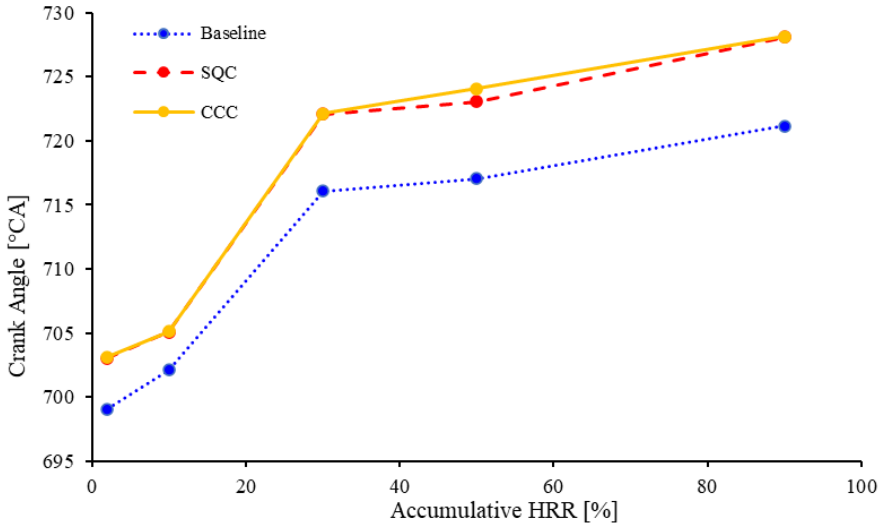

Figure 8. Comparison of accumulative heat release rate for different piston bowl geometries

4.0 CONCLUSIONS

The present study was designed to demonstrate the PFI-HCCI combustion engine in a numerical simulation approach on Yanmar L48N modified engine. During the simulation, the piston bowl volume, compression ratio, engine speed, and injected fuel mass were all held constant, allowing the results to be based solely on the geometry of the piston bowl. The simulation results were preliminary data study, starting from the intake valve open (IVO) to the exhaust valve close (EVC) at 2700 RPM engine speed. The findings reveal that:

i. The results indicate that in PFI-HCCI mode, the Baseline geometry exhibits the highest in-cylinder pressure of 8.46 MPa. In contrast, the SQC geometry demonstrates a pressure of 6.38 MPa, and the CCC geometry shows a pressure of 6.22 MPa. The modification of piston geometry leads to a decrease in in-cylinder pressure, reducing 24.6% for the SQC piston bowl geometry and 26.5% for the CCC piston bowl geometry.

ii. The average temperatures obtained in this study exhibited a correlation with the results of in-cylinder pressure. The Baseline geometry demonstrates the early onset of combustion prior to the TDC (715°CA), whereas the model for SQC and CCC display a certain degree of delay. The onset for both SQC and CCC geometries initiated at 720°CA.

iii. The Highest Heat Release Rate (HRR) of 34.88 J/°CA was obtained for the Baseline model, followed by SQC and CCC with HRR of 16.35 J/°CA and 15.50 J/°CA, respectively. According to the finding, the low-temperature kinetic reactions heat release curve is associated with the primary heat release curve.

iv. Results in this study reveal that the combustion with higher and shorter duration of HRR at earlier crank angle degree produced high in-cylinder pressure, thereby enhance the combustion.

v. In spite of its limitations, the present study offered the significant role of piston geometry for the control air-fuel mixing mechanism of PFI-HCCI combustion, which is a critical part of demonstrating HCCI combustion.

5.0 ACKNOWLEDGEMENTS

The authors appreciate Universiti Putra Malaysia for research facilities and grants. The study is supported by the GP-IPS research grant from UPM with project code GP-IPS 9706000 and in part by the Malaysia Fundamental Research Grant Scheme (FRGS) under grant 5524734.

6.0 REFERENCES

[1] P. Lyu, P. (Slade) Wang, Y. Liu, and Y. Wang, "Review of the studies on emission evaluation approaches for operating vehicles," *Journal of Traffic and Transportation Engineering (English Edition)*, vol. 8, no. 4, pp. 493–509, 2021.

[2] IEA, "Energy Technology Perspectives 2020," *Energy Technology Perspectives 2020, IEA, Paris*, 2020.

[3] L. Zhang, R. Long, H. Chen, and J. Geng, "A review of China's road traffic carbon emissions," *Journal of Cleaner Production*, vol. 207, pp. 569–581, 2019.

[4] ACEA, "Car and van CO2 targets: Europe needs a realistic roadmap to reach carbon neutrality," [Online]. Available: https://www.acea.auto (accessed Oct. 02, 2022).

[5] L. Xu *et al.*, "Effect of piston bowl geometry and compression ratio on in-cylinder combustion and engine performance in a gasoline direct-injection compression ignition engine under different injection conditions," *Applied Energy*, vol. 280, p. 115920, 2020.

[6] R. Kumar and M. Zheng, "Fuel efficiency improvements of low temperature combustion diesel engines," in *SAE Technical Papers*, no. 2008-01-0841, 2008.

[7] H. Bendu and M. Sivalingam, "Experimental investigation on the effect of charge temperature on ethanol fueled HCCI combustion engine," *Journal of Mechanical Science and Technology*, vol. 30, no. 10, pp. 4791–4799, 2016.

[8] M. Babagiray, T. Kocakulak, S. M. Safieddin Ardebili, H. Solmaz, C. Çınar, and A. Uyumaz, "Experimental and statistical investigation of different valve lifts on HCCI combustion, performance and exhaust emissions using response surface method," *Energy*, vol. 244, pp. 123184, 2022.

[9] H. M. Tobib, H. Rostam, M. A. A. Mossa, A. Aziz Hairuddin, and M. M. Noor, "The performance of an HCCI-DI engine fuelled with palm oil-based biodiesel," in *IOP Conference Series: Materials Science and Engineering*, vol. 469, p. 012079, 2019.

[10] M. Puškár and M. Kopas, "System based on thermal control of the HCCI technology developed for reduction of the vehicle NOX emissions in order to fulfil the future standard Euro 7," *Science of the Total Environment*, vol. 643, pp. 674–680, 2018.

[11] M. M. Hasan and M. M. Rahman, "Homogeneous charge compression ignition combustion: Advantages over compression ignition combustion, challenges and solutions," *Renewable and Sustainable Energy Reviews*, vol. 57, pp. 282–291, 2016.

[12] M. S. M. Alias, A. A. Hairuddin, M. K. Hassan, and K. A. M. Rezali, "A review of hydrogen addition in an HCCI engine fueled with biofuels," in *AIP Conference Proceedings*, vol. 2059, p. 020045, 2019.

[13] A. W. Gray and T. W. Ryan, "Homogeneous charge compression ignition (HCCI) of diesel fuel," in *SAE Technical Papers*, no. 971676, 1997.

[14] H. Liu, M. Yao, B. Zhang, and Z. Zheng, "Effects of inlet pressure and octane numbers on combustion and emissions of a homogeneous charge compression ignition (HCCI) engine," *Energy and Fuels*, vol. 22, no. 4, pp. 2207–2215, 2008.

[15] M. Christensen, A. Hultqvist, and B. Johansson, "Demonstrating the multi fuel capability of a homogeneous charge compression ignition engine with variable compression ratio," in *SAE Technical Papers*, no. 1999-01–3679, 1999.

[16] P. L. Kelly-Zion and J. E. Dec, "A computational study of the effect of fuel type on ignition time in homogeneous charge compression ignition engines," in *Proceedings of the Combustion Institute*, vol. 28, no. 1, pp. 1187–1194, 2000.

[17] M. Yao, Z. Zheng, and H. Liu, "Progress and recent trends in homogeneous charge compression ignition (HCCI) engines," *Progress in Energy and Combustion Science,* vol. 35, no. 5, pp. 398–437, 2009.

[18] J. V. Pastor, A. García, C. Micó, F. Lewiski, A. Vassallo, and F. C. Pesce, "Effect of a novel piston geometry on the combustion process of a light-duty compression ignition engine: An optical analysis," *Energy*, vol. 221, p. 119764, 2021.

[19] J. Benajes, A. García, J. M. Pastor, and J. Monsalve-Serrano, "Effects of piston bowl geometry on reactivity controlled compression ignition heat transfer and combustion losses at different engine loads," *Energy*, vol. 98, pp. 64–77, 2016.

[20] G. Mittal, M. Subhash, and M. Gwalwanshi, "Effect of initial turbulence on combustion with ECFM-3Z model in a CI engine," in *Materials Today: Proceedings*, vol. 46, no. 20, pp. 11007-11010, 2021.

[21] X. Wang and H. Zhao, "Effect of piston shape design on the scavenging performance and mixture preparation in a two-stroke boosted uniflow scavenged direct injection gasoline engine," *International Journal of Engine Research*, vol. 22, no. 5, pp. 1484–1499, 2021.

[22] I. H. Rizvi and R. Gupta, "Numerical investigation of injection parameters and piston bowl geometries on emission and thermal performance of DI diesel engine," *SN Applied Sciences*, vol. 3, no. 626, 2021.

[23] P. Prabhakaran, C. G. Saravanan, R. Vallinayagam, M. Vikneswaran, N. Muthukumaran, and K. Ashok, "Investigation of swirl induced piston on the engine characteristics of a biodiesel fueled diesel engine," *Fuel*, vol. 279, p. 118503, 2020.

[24] O. Adeniyi, "Numerical investigation on the effect of piston bowl geometry on combustion characteristics of a heavy-duty diesel engine," *Mapta Journal of Mechanical and Industrial Engineering (MJMIE)*, vol. 3, no. 2, pp. 9–20, 2019.

[25] C. P. Abdul Gafoor and R. Gupta, "Numerical investigation of piston bowl geometry and swirl ratio on emission from diesel engines," *Energy Conversion and Management*, vol. 101, pp. 541–551, 2015.

[26] John Heywood, Internal Combustion Engine Fundamentals, 2nd Ed. *McGraw-Hill Education*, 2018.

[27] C. D. Rakopoulos, G. M. Kosmadakis, and E. G. Pariotis, "Investigation of piston bowl geometry and speed effects in a motored HSDI diesel engine using a CFD against a quasi-dimensional model," *Energy Conversion and Management*, vol. 51, pp. 470–484, 2010.

[28] K. Zha, S. Busch, A. Warey, R. C. Peterson, and E. Kurtz, "A study of piston geometry effects on late-stage combustion in a light-duty optical diesel engine using combustion image velocimetry," *SAE International Journal of Engines*, vol. 11, no. 6, pp. 1-21, 2018.

[29] G. M. Shaver, J. C. Gerdes, and M. J. Roelle, "Physics-based modeling and control of residual-affected HCCI engines," *Journal of Dynamic Systems, Measurement and Control, Transactions of the ASME*, vol. 131, no. 2, p. 021002, 2009.

[30] M. A. Rather and M. M. Wani, "A numerical study on the effects of exhaust gas recirculation temperature on controlling combustion and emissions of a diesel engine running on HCCI combustion mode," *International Journal of Automotive Science And Technology*, vol. 2, no. 3, pp. 17–27, 2018.

[31] A. Turkcan, M. D. Altinkurt, G. Coskun, and M. Canakci, "Numerical and experimental investigations of the effects of the second injection timing and alcohol-gasoline fuel blends on combustion and emissions of an HCCI-DI engine," *Fuel*, vol. 219, pp. 50–61, 2018.

[32] M. Pourfallah, M. Armin, and A. A. Ranjbar, "A numerical study on the effect of thermal and charge stratification on the HCCI natural gas engine," *International Journal of Ambient Energy*, vol. 42, no. 12, pp. 1386–1395, 2021.

[33] Q. Deng and Q. Lin, "Numerical study of combustion in an HCCI fuelled with methane-hydrogen," *Journal of University of Science and Technology of China*, vol. 49, no. 6, pp. 476–486, 2019.

[34] H. Yu, X. Liang, and G. Shu, "Numerical study of the early injection parameters on wall wetting characteristics of an HCCI diesel engine using early injection strategy," *International Journal of Automotive Technology*, vol. 49, no. 6, pp. 476–486, 2017.

[35] T. K. Sharma, G. A. Prasad Rao, and K. M. Murthy, "Numerical investigations on HCCI engine with increased induction induced swirl and engine speed," *Journal of Central South University*, vol. 22, no. 10, pp. 3837–3848, 2015.

[36] H. M. Tobib, "Experimental investigation on performance of homogeneous charge compression ignition engine fueled with palm oil based biodiesel," *Master Thesis*, Universiti Putra Malaysia, Malaysia, 2019.

[37] Ansys, "Forte Theory Manual," *ANSYS Inc., USA*. 2021.

[38] A. Patel, S. C. Kong, and R. D. Reitz, "Development and validation of a reduced reaction mechanism for HCCI engine simulations," in *SAE Technical Papers*, no. 2004-01–0558, 2004.

[39] V. Yakhot and S. A. Orszag, "Renormalization group analysis of turbulence. I. Basic theory," *Journal of Scientific Computing*, vol. 1, no. 1, pp. 3–51, 1986.

[40] Ansys, "ANSYS Chemkin-Pro Theory Manual." ANSYS Inc., USA, 2022.

[41] P. R. Ganji, R. N. Singh, V. R. K. Raju, and S. Srinivasa Rao, "Design of piston bowl geometry for better combustion in direct-injection compression ignition engine," *Sadhana*, vol. 43, no. 92, pp. 1-9, 2018.

[42] N. A. Henein, A. Bhattacharyya, J. Schipper, A. Kastury, and W. Bryzik, "Effect of injection pressure and swirl motion on diesel engine-out emissions in conventional and advanced combustion regimes," in *SAE Technical Papers*, no. 2006-01–0076, 2006.

[43] M. Furutani, Y. Ohta, and K. Komatsu, "Onset behavior of autoignited low-temperature flames caused by piston compression," *Transactions of the Japan Society of Mechanical Engineers Series B*, vol. 59, no. 559, pp. 946–952, 1993.

[44] H. Liu, M. Yao, B. Zhang, and Z. Zheng, "Influence of fuel and operating conditions on combustion characteristics of a homogeneous charge compression ignition engine," in *Energy and Fuels*, vol. 23, pp. 1422–1430, 2009.